Electronic Supplementary Material

Germanium- and Tin-Bridged Diazulenylmethyl Cations: Effects of the Group 14 Elements on the Structure and Properties of π-Extended Cations

Masahito Murai,*[,†] Mako Ito,[†] Satoshi Takahashi,[†] and Shigehiro Yamaguchi*[,†,#]

[†]*Department of Chemistry, Graduate School of Science, and Integrated Research Consortium on Chemical Science (IRCCS), Nagoya University, Furo, Chikusa, Nagoya 464-8602, Japan*

[#]*Institute of Transformative Bio-Molecules (WPI-ITbM), Nagoya University Furo, Chikusa, Nagoya, 464-8601, Japan*

E-mail: masahito.murai@chem.nagoya-u.ac.jp
yamaguchi@chem.nagoya-u.ac.jp

Table of Contents

1. Synthetic Procedures

General. All reactions were performed in dry solvents under a nitrogen atmosphere. Anhydrous THF and CH_2Cl_2 were purchased from Kanto Chemicals and further purified by Glass Contour Solvent Systems. Anhydrous cyclohexane, MeOH, and DMF were purchased from Kanto Chemicals. Unless otherwise noted, other chemicals obtained from commercial suppliers were used without further purification. 2-Iodoazulene was prepared according to the reported procedure.[S1] ^{1}H (400 MHz), ^{13}C (100 or 150 MHz), ^{19}F (376 MHz) and ^{31}P (162 MHz) NMR spectra were recorded with a JEOL JNM-AL400 spectrometer, JEOL JNM-ECS400 spectrometer, and JEOL ECA 600 II spectrometer equipped with a UltraCOOL probe. The chemical shifts in ^{1}H NMR spectra were reported in ppm based on the solvent resonance resulting from incomplete deuteration ($CHCl_3$ at 7.26 ppm or CH_3OH at 3.31 ppm) as the internal standard. ^{13}C NMR spectra were recorded with complete proton decoupling, and the chemical shifts were reported in ppm relative to $CDCl_3$ at 77.16 ppm or CD_3OD at 49.00 ppm as internal standards. The chemical shifts in ^{31}P NMR and ^{19}F NMR were reported using H_3PO_4 (at 0.00 ppm) and CF_3COOH (at −76.5 ppm) as external standards, respectively. The following abbreviations are used; s: singlet, d: doublet, t: triplet, q: quartet, sept: septet. High-resolution mass spectra (HRMS) were measured with a Thermo Fisher Scientific Exactive Spectrometer with the ESI ionization method, and a Bruker microTOF Focus spectrometry system with the ionization method of APCI. Thin layer chromatography (TLC) was performed on glass plates coated with 0.25 mm thickness of silica gel $60F_{254}$ (Merck). Column chromatography was performed using silica gel PSQ60B (Fuji Silysia Chemicals). Melting points (Mp) were measured on a Yanaco micromelting point apparatus (MP-S3), and are uncorrected.

Di(2-azulenyl)dimethylgermane (4). A solution of 2-iodoazulene[S1] (100 mg, 0.394 mmol) in Et_2O (0.8 mL) was added *n*-BuLi (1.6 M in hexane, 0.25 mL, 0.40 mmol) dropwise over a period of 2 min at –78 °C followed by stirring for 1 h. Dichlorodimethylgermane (23 μL, 0.20 mmol) was added at –78 °C, and the resulting mixture was stirred at the same temperature for 1 h. After further stirred at room temperature for 3 h, H_2O (5 mL) was added and the mixture was

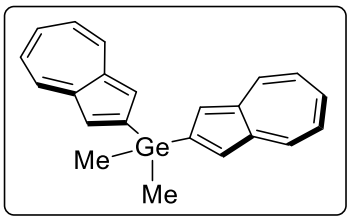

extracted with CH_2Cl_2 (10 mL) three times. The combined organic layer was washed with a saturated aqueous solution of NaCl (20 mL), dried over Na_2SO_4, and filtered. The volatiles were removed under reduced pressure, and the resulting mixture was subjected to flash column chromatography on silica gel using 10/3 hexane/CH_2Cl_2 (R_f = 0.50) as eluent to afford 64.0 mg (0.179 mmol, 91% yield) of **4** as a blue solid. Mp: 128.2–129.3 °C. ^{1}H NMR (400 MHz, $CDCl_3$): δ 8.30 (d, J = 9.6 Hz, 4H), 7.58 (s, 4H), 7.57 (t, J = 9.6 Hz, 2H), 7.15 (t, J = 9.6 Hz, 4H), 0.85 (s, 6H). ^{13}C{^{1}H} NMR (100 MHz, $CDCl_3$): δ 152.6, 140.6, 137.6, 136.1, 123.9, 123.0, –1.7. HRMS (APCI): m/z calcd. for $C_{22}H_{20}Ge$ ($[M]^+$) 358.0771, found 358.0770.

Compound $\mathbf{2_{Cl}}$. To a solution of **4** (39.1 mg, 0.110 mmol) in DMF (4.5 mL) was added $POCl_3$ (22 μL, 0.24 mmol), and the resulting mixture was stirred at 60 °C for 3 h. After cooling to room temperature, H_2O (2 mL) was added and the mixture was extracted with CH_2Cl_2 (20 mL) three times. The combined organic layer was washed with a saturated aqueous solution of NaCl (30 mL), dried over Na_2SO_4, and filtered. The volatiles were removed under reduced pressure, and the resulting mixture was washed with hexane to afford 36.9 mg (0.0914 mmol, 83% yield) of $\mathbf{2_{Cl}}$ as a blue solid. ^{1}H NMR (400 MHz, CD_3OD): δ 9.60 (s, 1H), 9.53 (d, J = 9.6 Hz, 2H), 8.81 (d, J = 9.6 Hz, 2H), 8.33 (t, J = 9.6 Hz, 2H), 8.20 (t, J = 9.6 Hz, 2H), 8.12 (t, J = 9.6 Hz, 2H), 8.11 (s, 2H), 0.84 (s, 6H). ^{13}C{^{1}H} NMR (100 MHz, CD_3OD): δ 157.8, 154.3, 152.0, 144.9, 141.8, 139.6, 138.1, 138.0, 136.43, 136.36, 135.6, –1.0. HRMS (ESI): m/z calcd. for $C_{23}H_{19}Ge$ ($[M–Cl]^+$) 369.0693, found 369.0693.

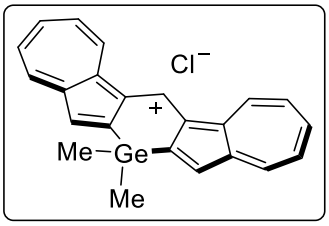

Compound $\mathbf{2_{PF6}}$. To a solution of $\mathbf{2_{Cl}}$ (131 mg, 0.324 mmol) in MeOH (9.2 mL) and H_2O (9.2 mL) was added KPF_6 (339 mg, 1.84 mmol), and the resulting mixture was stirred at room temperature for 17 h. After removal of MeOH under reduced pressure, the mixture was successively washed with H_2O and hexane to afford 146 mg (0.284 mmol, 88% yield) of $\mathbf{2_{PF6}}$ as a blue solid. ^{1}H NMR (400 MHz, CD_3OD): δ 9.59 (s, 1H), 9.52 (d, J = 9.6 Hz, 2H), 8.80 (d, J = 9.6 Hz, 2H), 8.32

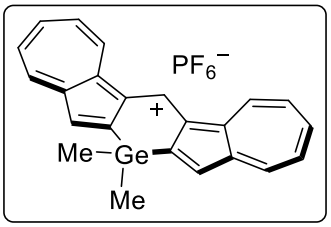

(d, J = 9.6 Hz, 2H), 8.19 (t, J = 9.6 Hz, 2H), 8.12 (t, J = 9.6 Hz, 2H), 8.11 (s, 2H), 0.84 (s, 6H). $^{13}C\{^{1}H\}$ NMR (150 MHz, CD_3OD): δ 158.0, 154.4, 152.1, 144.8, 141.7, 139.5, 138.0 (two peaks overlapped), 136.3 (two peaks overlapped), 135.6, –0.98. ^{19}F NMR (376 MHz, CD_3OD): δ –73.9 (d, $J_{F–P}$ = 710.0 Hz). $^{31}P\{^{1}H\}$ NMR (162 MHz, CD_3OD): δ –143.9 (sept, $J_{P–F}$ = 710.0 Hz). HRMS (ESI): m/z calcd. for $C_{23}H_{19}Ge$ ($[M–PF_6]^+$) 369.0693, found 369.0693.

Di(2-azulenyl)dimethylstannane (5). A solution of 2-iodoazulene[S1] (150 mg, 0.590 mmol) in Et_2O (3.4 mL) was added *n*-BuLi (1.6 M in hexane, 0.37 mL, 0.59 mmol) dropwise over a period of 2 min at –78 °C followed by stirring for 1 h. Dichlorodimethylstannane (65.0 mg, 0.296 mmol) was added at –78 °C, and the resulting mixture was stirred at room temperature for 4 h. After addition of H_2O (10 mL), the mixture was extracted with CH_2Cl_2 (15 mL) three times. The combined organic layer was washed with a saturated aqueous solution of NaCl (20 mL), dried over Na_2SO_4, and filtered. The volatiles were removed under reduced pressure, and the resulting mixture was subjected to flash column chromatography on silica gel using 9/1 hexane/CH_2Cl_2 (R_f = 0.43) as the eluent to afford 59.1 mg (0.146 mmol, 49% yield) of **5** as a blue solid. Mp: 142.1–142.8 °C. ^{1}H NMR (400 MHz, $CDCl_3$): δ 8.30 (d, J = 9.6 Hz, 4H), 7.63 (t, $J_{H–Sn}$ = 21.2 Hz, 4H), 7.57 (t, J = 9.6 Hz, 2H), 7.16 (t, J = 9.6 Hz, 4H), 0.67 (t, $J^{117/119}_{H–Sn}$ = 58.0/55.6 Hz, 6H). $^{13}C\{^{1}H\}$ NMR (100 MHz, $CDCl_3$): δ 152.0, 140.4, 137.6, 135.7, 126.3, 122.9, –9.1. HRMS (APCI): m/z calcd. for $C_{22}H_{20}Sn$ ($[M]^+$) 404.0581, found 404.0584.

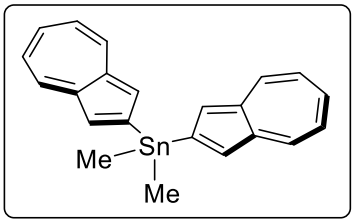

Compound 3Cl. To a solution of **5** (101 mg, 0.249 mmol) in DMF (10 mL) was added $POCl_3$ (45 μL, 0.49 mmol), and the resulting mixture was stirred at 0 °C for 1.5 h. H_2O (1 mL) was added at room temperature and the mixture was extracted with CH_2Cl_2 (20 mL) seven times. The combined organic layer was washed with a saturated aqueous solution of NaCl (125 mL), dried over Na_2SO_4, and filtered. The volatiles were removed under reduced pressure, and the

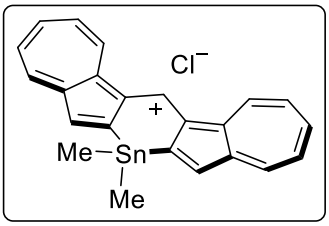

resulting mixture was washed with hexane to afford 20.6 mg (0.0414 mmol, 17% yield) of **3$_{Cl}$** as a blue solid. ^{1}H NMR (400 MHz, CD_3OD): δ 9.57 (d, J = 9.6 Hz, 2H), 9.55 (s, 1H), 8.75 (d, J = 9.6 Hz, 2H), 8.29 (t, J = 9.6 Hz, 2H), 8.161 (t, J = 9.6 Hz, 2H), 8.159 (s, 2H), 8.09 (t, J = 9.6 Hz, 2H), 0.72 (t, $J^{117/119}_{H–Sn}$ = 67.2/64.4 Hz, 6H). ^{13}C{^{1}H} NMR (100 MHz, CD_3OD): δ 161.2, 154.0, 152.9, 144.4, 140.9, 139.9, 139.4, 137.8, 137.2, 136.7, 135.8, –7.3. HRMS (ESI): *m*/*z* calcd. for $C_{23}H_{19}Sn$ ([M–Cl]$^+$) 415.0503, found 415.0499.

Compound 3$_{PF6}$. To a solution of **3$_{Cl}$** (14.8 mg, 0.0297 mmol) in MeOH (0.9 mL) and H_2O (0.9 mL) was added KPF_6 (33.6 mg, 0.182 mmol), and the resulting mixture was stirred at room temperature for 12 h. After removal of MeOH under reduced pressure, the mixture was successively washed with H_2O and hexane to afford 11.0 mg (0.0196 mmol, 66% yield) of **3$_{PF6}$** as a blue solid. ^{1}H NMR (400 MHz, CD_3OD): δ 9.56 (d, J = 9.6 Hz, 2H), 9.55 (s, 1H), 8.75 (d, J = 9.6 Hz, 2H), 8.29 (d, J = 9.6 Hz, 2H), 8.17 (t, J = 9.6 Hz, 2H), 8.16 (s, 2H), 8.09 (t, J = 9.6 Hz, 2H), 0.72 (t, $J^{117/119}_{H–Sn}$ = 65.6/64.8 Hz, 6H). ^{13}C{^{1}H} NMR (150 MHz, CD_3OD): δ 161.2, 154.0, 152.9, 144.4, 140.9, 139.9, 139.4, 137.8, 137.2, 136.7, 135.8, –7.3. ^{19}F NMR (376 MHz, CD_3OD): δ –74.1 (d, $J_{F–P}$ = 713.6 Hz). ^{31}P{^{1}H} NMR (162 MHz, CD_3OD): δ –143.9 (sept, $J_{P–F}$ = 713.6 Hz). HRMS (ESI): *m*/*z* calcd. for $C_{23}H_{19}Sn$ ([M–PF_6]$^+$) 415.0503, found 415.0502.

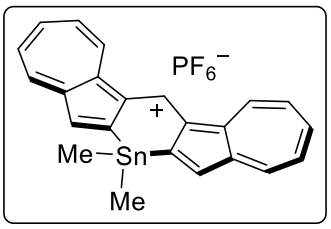

2. Determination of pK_R^+ Values

K_R^+ is an equilibrium constant for the reaction shown in eq S1 in an aqueous solution and pK_R^+ is defined by eq S2, and. The pK_R^+ values were determined according to the literature method.[S2] Thus, a solution of **2$_{PF6}$** or **3$_{PF6}$** in DMSO was added to aqueous buffers with varied pH values. Citric acid/Na_2HPO_4 (for pH = 3–7), $(H_2N)C(CH_2OH)_3$/HCl (pH = 7–9), Na_2CO_3/$NaHCO_3$ (pH = 9–11), Na_2HPO_4/NaOH (pH = 11–12), and NaOH/KCl (pH = 12–13) were used to prepare the aqueous buffer solutions, and the solution mixtures were left at room temperature for 10 min in the dark prior to the measurement. The relative absorbance of **2$_{PF6}$** and **3$_{PF6}$** at the longest absorption band were plotted against the pH values, and the resulting plots were analyzed by non-linear least square curve fitting using eq S3, where A_0 and A_∞ represent the initial and final

absorbance values at 646 nm, respectively (Figure S1). Based on this procedure, the pK_R^+ values were determined to be 10.5 (R^2 = 0.95417) for **2**$_{PF6}$, and 11.5 (R^2 = 0.99351) for **3**$_{PF6}$. The pK_R^+ values of **1**$_{PF6}$ and trioxatriangulenium hexafluorophosphate, [TOTA][PF_6], were determined to be 9.7 and 9.3, which was consistent with the reported values.[S1a,2]

$$R^+ + H_2O \rightleftharpoons ROH + H^+ \qquad \text{(S1)}$$

$$K_R^+ = \frac{[ROH]\,[H^+]}{[R^+]} \quad \text{hence} \quad pK_R^+ = pH - \log\frac{[ROH]}{[R^+]} \qquad \text{(S2)}$$

$$A = \frac{A_0 \cdot 10^{-pH} + A_\infty \cdot 10^{-pK_R^+}}{10^{-pH} + 10^{-pK_R^+}} \qquad \text{(S3)}$$

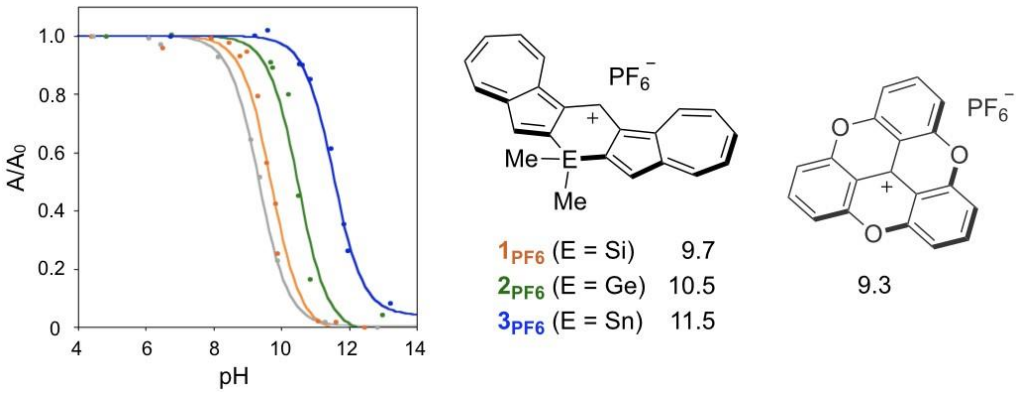

Figure S1. Plots of absorbance change of **1**$_{PF6}$ (orange), **2**$_{PF6}$ (green), **3**$_{PF6}$ (blue), and [TOTA][PF_6] (grey) in 1 vol% of DMSO in aqueous buffer as a function of pH values and their fitting curves.

3. Theoretical Calculations

All quantum calculations were performed using the Gaussian 16 program.[S3] The

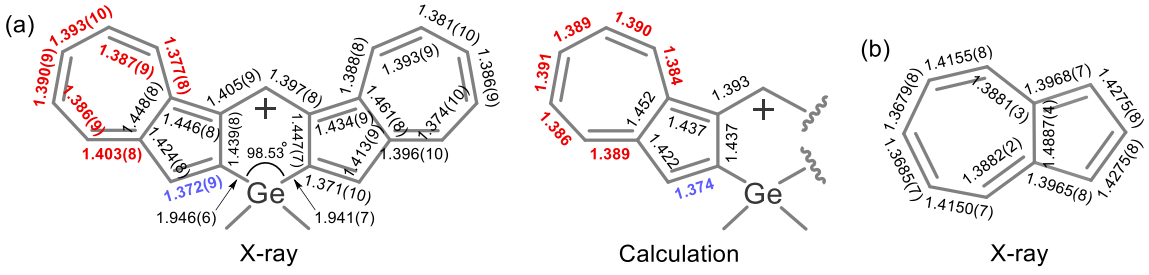

Figure S2. (a) Bond lengths of **2**$_{PF6}$ obtained from X-ray single crystal analysis and DFT calculations. The unit cell contains two crystallographically independent molecules, and the data for one of those geometries are shown here. (b) Bond lengths in azulene determined by X-ray crystallographic analysis.[S4]

geometry optimized at the M06/6-311+G(d,p) level of theory were used for the TD-DFT calculations at the same level of theory. The Cartesian coordinates for **2** and **3** are shown in Table S1.

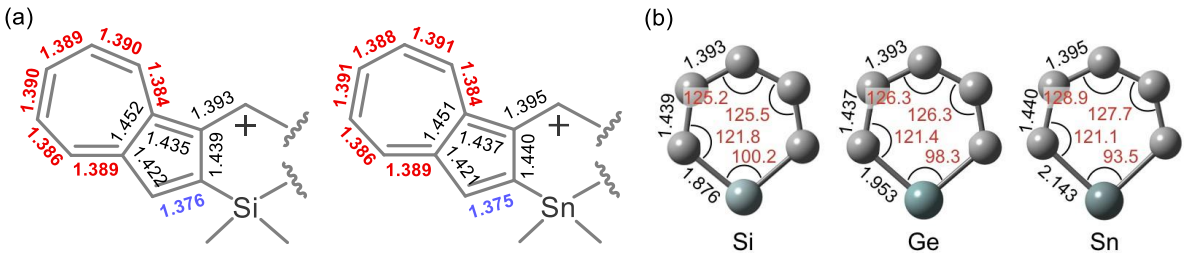

Figure S3. (a) Bond lengths and (b) angles of the optimized structures calculated at the M06/6-311+G(d,p) (for Si, Ge, C, H) and LANL2DZ (for Sn) level of theories.

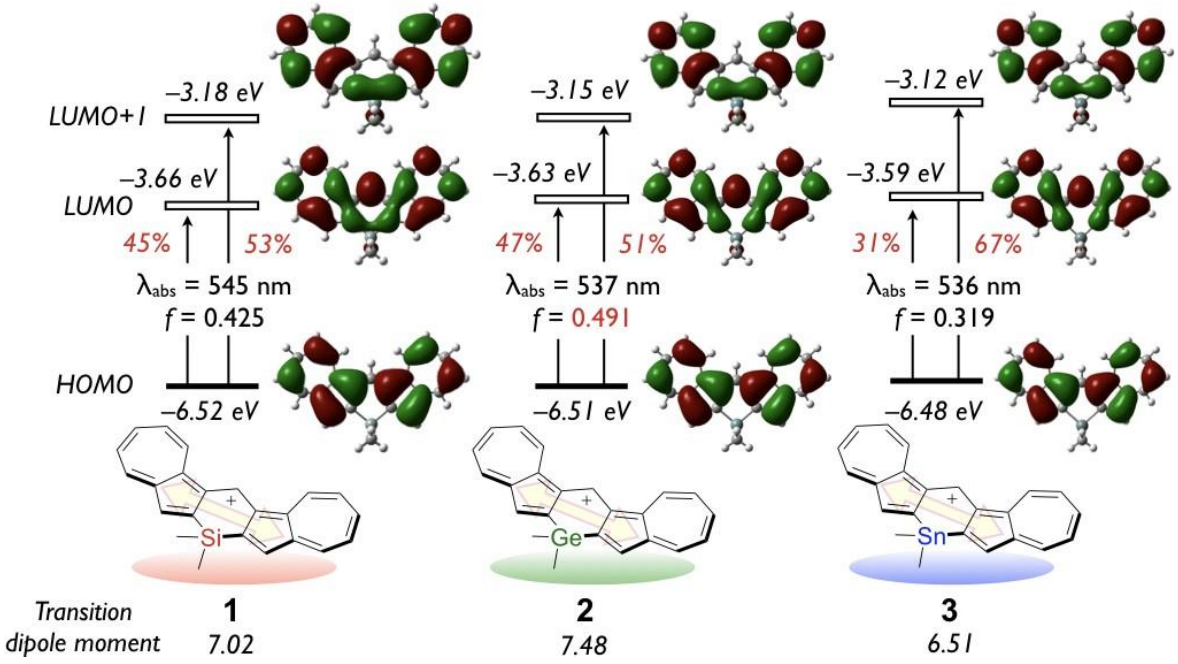

Figure S4. Kohn−Sham molecular orbitals (isovalue: 0.017) and electronic transitions of **1**, **2**, and **3** calculated at the M06/6-311+G(d,p) (for Si, Ge, C, H) and LANL2DZ (for Sn) level of theories with CH_2Cl_2 using the polarizable continuum model (PCM). Values in red are the percentage of transition probabilities in S_0–S_1. Arrows on the chemical structures indicate the direction of the transition dipole moments.

Table S1. Cartesian coordinates for **2** and **3** optimized at the M06/6-311+G(d,p) (for Si, Ge, C, H) and LANL2DZ (for Sn) level of theories.

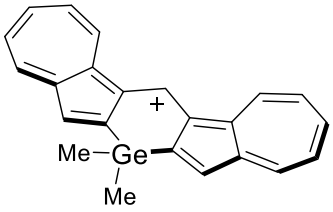

2

	X	Y	Z
C	-1.24289914	-0.41880634	0.00000027
C	-2.51932649	-1.07963791	-0.00000058
C	0.00000259	-1.04805948	0.0000083
C	-1.47805056	0.99894249	-0.00000836
Ge	-0.0000007	2.27601343	0.0000063
C	1.24290236	-0.41880201	0.00000622
C	1.47805373	0.99894749	-0.00000472
C	-2.83554974	1.21442016	-0.00001666
C	-0.00000364	3.36146162	-1.61559416
H	0.00000496	-2.13718662	0.00001598
C	2.51933021	-1.07963296	0.00000377
C	-2.73030341	-2.44696254	0.0000068
C	-3.52335193	-0.0303617	-0.00001258
H	-3.3376255	2.17559386	-0.00002534
C	-4.90638609	-0.16145886	-0.00001963
H	-1.84031827	-3.07306153	0.0000151
C	-3.93543573	-3.14138425	0.00000477
C	-5.23076477	-2.64222596	-0.00000531
H	-3.85024976	-4.2244698	0.00001197
H	-6.01807488	-3.39198177	-0.00000448
H	-5.46161002	0.77506879	-0.00002865
C	-5.66621276	-1.32102337	-0.00001626
H	-6.74346793	-1.17981783	-0.00002302
C	2.73030889	-2.44695735	0.00001651
C	3.52335535	-0.03035665	-0.0000151
C	2.83555281	1.21442497	-0.00002033
C	4.90638961	-0.16145233	-0.00002587
C	5.66621784	-1.32101583	-0.00001872
H	5.46161235	0.77507605	-0.00004098
C	5.23077094	-2.64221875	0.00000024
H	6.74347285	-1.17980893	-0.00002897
H	6.01808144	-3.39197416	0.00000327
H	1.84032488	-3.07305798	0.00003003
C	3.93544195	-3.14137777	0.00001556
H	3.3376284	2.17559867	-0.00003363
H	3.85025659	-4.22446336	0.00002878
C	-0.00002534	3.36140513	1.61564569
H	-0.88901895	3.99721979	1.63159307
H	-0.00000473	2.72282153	2.50121016
H	0.88892512	3.99727959	1.63159325
H	-0.00000689	2.7229122	-2.50118306
H	-0.88897554	3.99730727	-1.63151365
H	0.88896791	3.99730747	-1.63152041

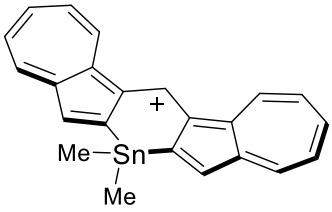

3

	X	Y	Z
C	-1.25820863	-0.6165713	0.00001719
C	-2.50504141	-1.33844534	0.00000072
C	-0.00000047	-1.21807586	0.00002838
C	-1.56053909	0.79144247	-0.00000176
Sn	0.00000043	2.26037561	-0.0000054
C	1.25820814	-0.61657209	0.00001999
C	1.56053856	0.79144149	0.00000251
C	-2.92814343	0.93536188	0.00001864
C	0.00001098	3.42179688	-1.78235367
H	-0.00000086	-2.30720011	0.00001442
C	2.50504069	-1.33844625	0.00000268
C	-2.65803373	-2.71361433	-0.00000441
C	-3.55743015	-0.33892209	0.00000144
H	-3.47917531	1.86907615	0.00003038
C	-4.93345011	-0.53059501	-0.00000071
H	-1.7437079	-3.3033226	-0.00000406
C	-3.83194799	-3.46037505	-0.00000775
C	-5.1486377	-3.02166287	-0.00000799
H	-3.69738724	-4.53859523	-0.00001154
H	-5.90060859	-3.8068486	-0.00001348
H	-5.52776025	0.38174749	0.0000026
C	-5.64302442	-1.72124741	-0.00000465
H	-6.72547114	-1.62730845	-0.0000069
C	2.65803265	-2.71361528	-0.0000026
C	3.5574296	-0.33892298	0.00000375
C	2.92814296	0.93536099	0.00002241
C	4.93344948	-0.53059626	0.00000066
C	5.64302347	-1.72124889	-0.00000447
H	5.52775988	0.38174606	0.000004
C	5.1486365	-3.02166422	-0.00000802
H	6.72547024	-1.62731016	-0.0000075
H	5.90060727	-3.80685008	-0.00001447
H	1.7437066	-3.30332321	-0.00000143
C	3.83194673	-3.46037626	-0.00000684
H	3.47917481	1.86907529	0.00003472
H	3.69738583	-4.53859642	-0.00001062
C	-0.00000733	3.4218071	1.78233611
H	-0.88779071	4.0574687	1.81474761
H	-0.00001828	2.76577649	2.65502668
H	0.88778208	4.05745946	1.81476276
H	0.0000121	2.76576141	-2.65504056
H	-0.8877724	4.05745779	-1.81478009
H	0.8878004	4.05744985	-1.81477217

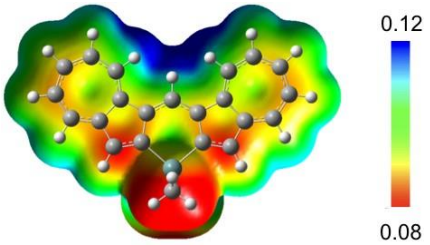

Figure S5. Electrostatic potential (ESP) map of **2** calculated at the M06/6-311+G(d,p) level of theory without including a counter anion

All theoretical calculations were conducted without including the counter anion, PF_6^-, because effects toward the bond lengths of optimized structures of cationic π-skeletons as well as the electronic transitions are very small as demonstrated in Figure S6. DFT calculations here were conducted at the M06/6-311+G(d,p) level for **1**$_{PF6}$ and **2**$_{PF6}$, the initial coordinates of which were taken from their crystal packing structures in Figure 2a and ref S1a.

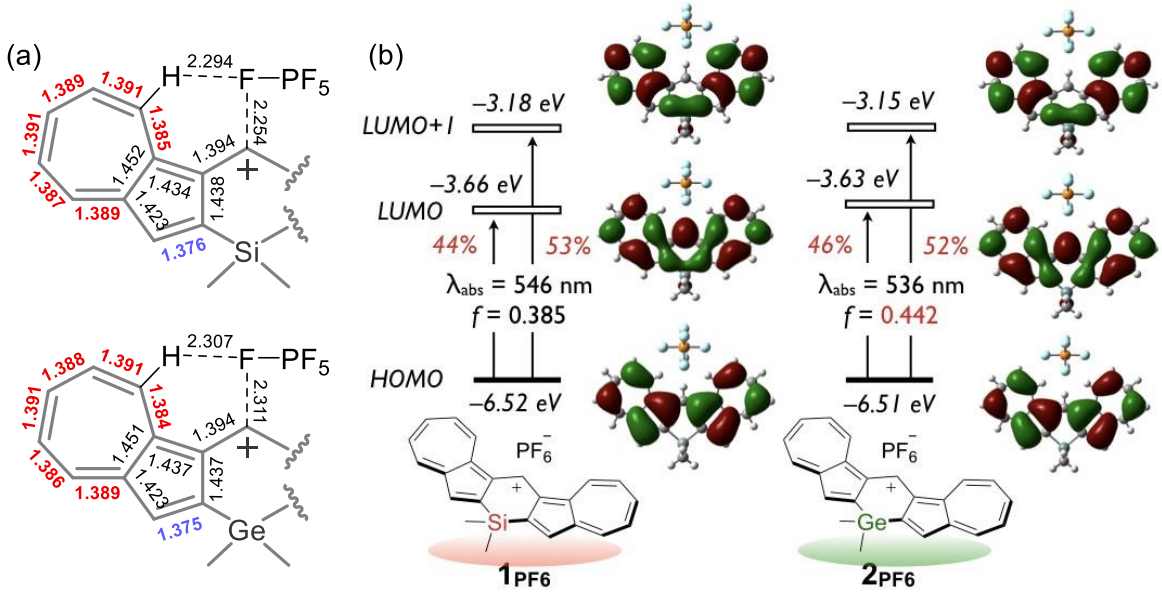

Figure S6. (a) Bond lengths of the optimized structures calculated at the M06/6-311+G(d,p) level of theories, and (b) Kohn−Sham molecular orbitals (isovalue: 0.017) and electronic transitions of **1**$_{PF6}$ and **2** $_{PF6}$ calculated at the M06/6-311+G(d,p) level of theories with CH_2Cl_2 using the polarizable continuum model (PCM). Values in red are the percentage of transition probabilities in S_0–S_1.

4. X-ray Crystallographic Analysis of $\mathbf{2}_{PF6}$.

Plate-shaped blue crystals suitable for X-ray analysis were obtained by slow evaporation of a solution of $\mathbf{2}_{PF6}$ in CH_2Cl_2/hexane at room temperature. A crystal selected for X-ray experiment was a small block with dimensions of 0.01 mm×0.01 mm×0.01 mm. The intensity data were collected at 90 K on synchrotron radiation (λ = 0.4148 Å) at the BL02B1 beamline in SPring-8 (JASRI). A total of 9517 reflections were measured with the maximum 2θ angle of 31.1°, of which 9049 were independent reflections (R_{int} = 0.0999). The structure was solved by direct methods (SHELXS-2018/2) and refined by the full-matrix least-squares procedures on F^2 for all reflections (SHELXL-2018/3). Hydrogen atoms were placed using AFIX instructions, and all the other atoms were refined anisotropically. ORTEP diagrams are shown in Figures 2 and S7. The crystal data are as follows: $C_{23}H_{19}F_6GeP$; M_W = 512.94, monoclinic, space group *C*c, a = 29.1631(6) Å, b = 11.2974(2) Å, c = 13.8266(3) Å, α = 90°, β = 114.072(2)°, γ = 90°, V = 4159.24(16) Å^3 , Z = 8, D_{calcd} = 1.638 g cm^{-3}, μ = 0.378 mm^{-1}, F(000) = 2064. The refinement converged to R_1 [I>2σ(I)] = 0.0442, wR_2 (all data) = 0.0972, Goodness of Fit = 1.060. Crystallographic data have been deposited in the Cambridge Crystallographic Data Centre (CCDC) as supplementary publication No. CCDC-2252079 for $\mathbf{2}_{PF6}$, which can be obtained free of charge *via* www.ccdc.cam.ac.uk/data_request/cif.

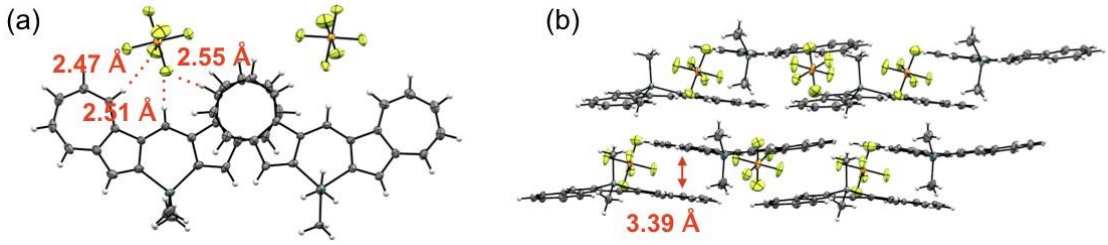

Figure S7. (a) A top view of the neighboring two molecules and (b) a side view of the molecular arrangement in the crystal packing of $\mathbf{2}_{PF6}$ with the thermal ellipsoids drawn at 50% probability level. Blue: Ge, black: C, orange: P, and yellow: F. The shortest distances for the F···H–C hydrogen bonds and the shortest C···C distance in the adjacent two seven-membered rings are shown.

5. Cyclic Voltammetry (CV) Measurements

The measurements of CV were performed with an ALS/chi-617A electrochemical analyzer and the cyclic voltammograms are shown in Figure S8. The CV cell consisted of a glassy carbon electrode, a platinum wire counter electrode, and a $Ag/AgNO_3$ reference electrode was used. The measurements were carried out under an argon atmosphere using a CH_2Cl_2 solution of a sample with a concentration of 1 mM at a scan rate of 50 mV/s. Tetrabutylammonium hexafluorophosphate [*n*-Bu_4N][PF_6] was used as a supporting electrolyte with a concentration of 0.1 M. The redox potentials were calibrated against a ferrocene/ferrocenium (Fc/Fc^+) couple.

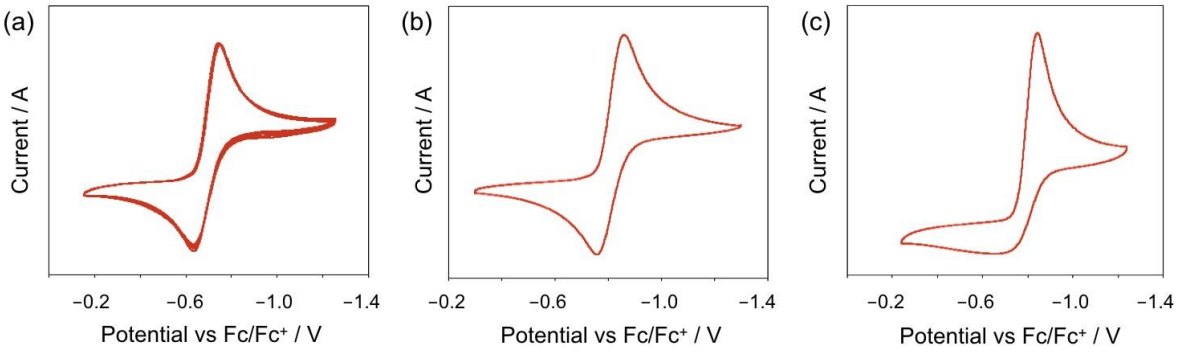

Figure S8. Cyclic voltammograms of (a) **1**$_{PF6}$, (b) **2**$_{PF6}$, and (c) **3**$_{PF6}$ in CH_2Cl_2 (1.0×10^{-3} M) with *n*-Bu_4NPF_6 (0.1 M) as a supporting electrolyte at a scan rate of 50 mV/s. All potentials are calibrated with Fc/Fc^+.

6. Photophysical Properties

UV-vis absorption spectra were recorded on a Shimadzu UV-3150 spectrometer with a resolution of 0.2 nm using diluted sample solutions in spectral grade solvents. Quartz cuvettes with an optical path length of 1.0 cm were used for the measurements. Emission spectra were recorded on a HORIBA SPEX Fluorolog-3 spectrofluorometer (detection limit up to 1100 nm) equipped with a Hamamatsu PMA R5509-73 and a cooling system C9940-01 with a resolution of 1.0 nm. The measurement parameters for sensitivity, scanning rates, and ranges were chosen appropriately for each experiment. Absolute fluorescence quantum yields were determined with a Quantaurus-QY Plus C-13534-02 (Hamamatsu Photonics) equipped with NIR PL measurement unit C13684-01 calibrated with an integrating sphere system. The absorption spectra are shown in Figure 3a and

photophysical data are summarized in Table S2. These measurements were performed under dilute conditions to avoid the formation of aggregates.

Table S2. Summary of absorption properties in various solvents [a]

Compound	solvent	λ_{abs} / nm	ε / 10^4 $M^{-1}cm^{-1}$
$\mathbf{1}_{PF6}$	CH_2Cl_2	646	8.82
$\mathbf{2}_{PF6}$	CH_2Cl_2	639	11.8
$\mathbf{2}_{PF6}$	THF	634	9.20
$\mathbf{3}_{PF6}$	CH_2Cl_2	637	8.20

[a] Only the longest absorption maximum wavelengths are shown.

7. Photophysical Properties in the Aggregation State

A solution of a sample in 1,2-dichloroethane (DCE) was slowly injected into methylcyclohexane (MCH) at room temperature in the air so as to give a solution with a total concentration of *ca.* 1×10^{-5} M. After shaking gently, the UV-vis-NIR absorption change was monitored at room temperature on a Shimadzu UV-3150 spectrometer. The absorption spectra changes are shown in Figures 4a-c.

8. X-Ray Powder Diffraction Analysis of $\mathbf{2}_{PF6}$

A solution of $\mathbf{2}_{PF6}$ in DCE was diluted with cyclohexane so as to give a solution of $\mathbf{2}_{PF6}$ in 10/90 DCE/cyclohexane (*v*/*v*) with a total concentration of 1×10^{-5} M. After shaking gently, formation of the aggregates showing the longest absorption band at 773 nm was confirmed by UV-vis-NIR absorption spectra. After the volatiles were removed by freeze dry, the resulting black powder was used for the measurement of the X-ray powder diffraction analysis. Powder X-ray diffraction (XRD) pattern is shown in Figure S9.

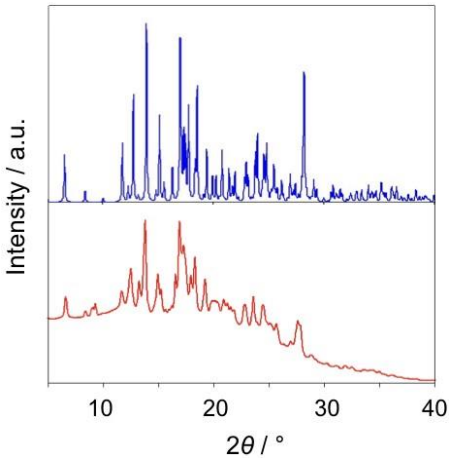

Figure S9. Powder X-ray diffraction (XRD) pattern of the aggregates of $\mathbf{2}_{\mathbf{PF6}}$ (red lines in the bottom layer). The blue line in the upper layer is the simulated pattern obtained from the analysis of single crystals.

9. References

S1. (a) M. Murai, M. Abe, S. Ogi, S. Yamaguchi, *J. Am. Chem. Soc.* 2022, **144**, 20385. (b) M. Narita, T. Murafuji, S. Yamashita, M. Fujinaga, K. Hiyama, Y. Oka, F. Tani, S. Kamijo, K. Ishiguro, *J. Org. Chem.* 2018, **83**, 1298.

S2. (a) B. W. Laursen, F. C. Krebs, *Chem. –Eur. J.* 2001, **7**, 1773; (b) J. Bosson, J. Gouin, J. Lacour, *Chem. Soc. Rev.* 2014, **43**, 2824.

S3. M. J. Frisch, G. W. Trucks, H. B. Schlegel, G. E. Scuseria, M. A. Robb, J. R. Cheeseman, G. Scalmani, V. Barone, G. A. Petersson, H. Nakatsuji, X. Li, M. Caricato,A. V. Marenich, J. Bloino, B. G. Janesko, R. Gomperts, B. Mennucci, H. P. Hratchian, J. V. Ortiz, A. F. Izmaylov, J. L. Sonnenberg, D. Williams-Young, F. Ding, F. Lipparini, F. Egidi, J. Goings, B. Peng, A. Petrone, T. Henderson, D. Ranasinghe, V. G. Zakrzewski, J. Gao, N. Rega, G. Zheng, W. Liang, M. Hada, M. Ehara, K. Toyota, R. Fukuda, J. Hasegawa, M. Ishida, T. Nakajima, Y. Honda, O. Kitao, H. Nakai, T. Vreven, K. Throssell, J. A. Montgomery, Jr. J. E. Peralta, F. Ogliaro, M. J. Bearpark, J. J. Heyd, E. N. Brothers, K. N. Kudin, V. N. Staroverov, T. A. Keith, R. Kobayashi, J. Normand, K. Raghavachari, A. P. Rendell, J. C. Burant, S. S. Iyengar, J. Tomasi, M. Cossi, J. M. Millam, M. Klene, C. Adamo, R. Cammi, J. W. Ochterski, R. L. Martin, K. Morokuma, O. Farkas, J. B. Foresman, D. J. Fox, Gaussian Inc., Wallingford CT, 2016.

S4. B. Dittrich, F. P. A. Fabbiani, J. Henn, M. U. Schmidt, P. Macchi, K. Meindl, M. A. Spackman, *Acta Crystallogr., Sect. B: Struct. Sci., Cryst. Eng. Mater.* 2018, **74**, 416.

10. NMR Spectra of New Compounds

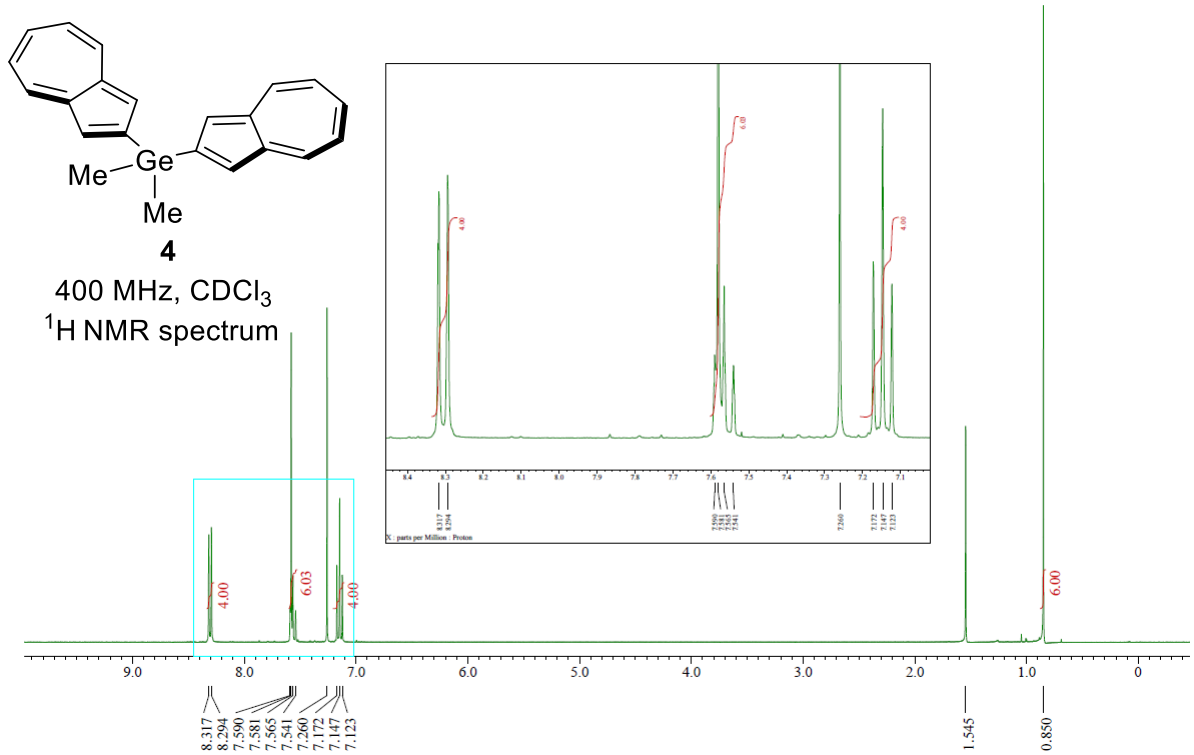

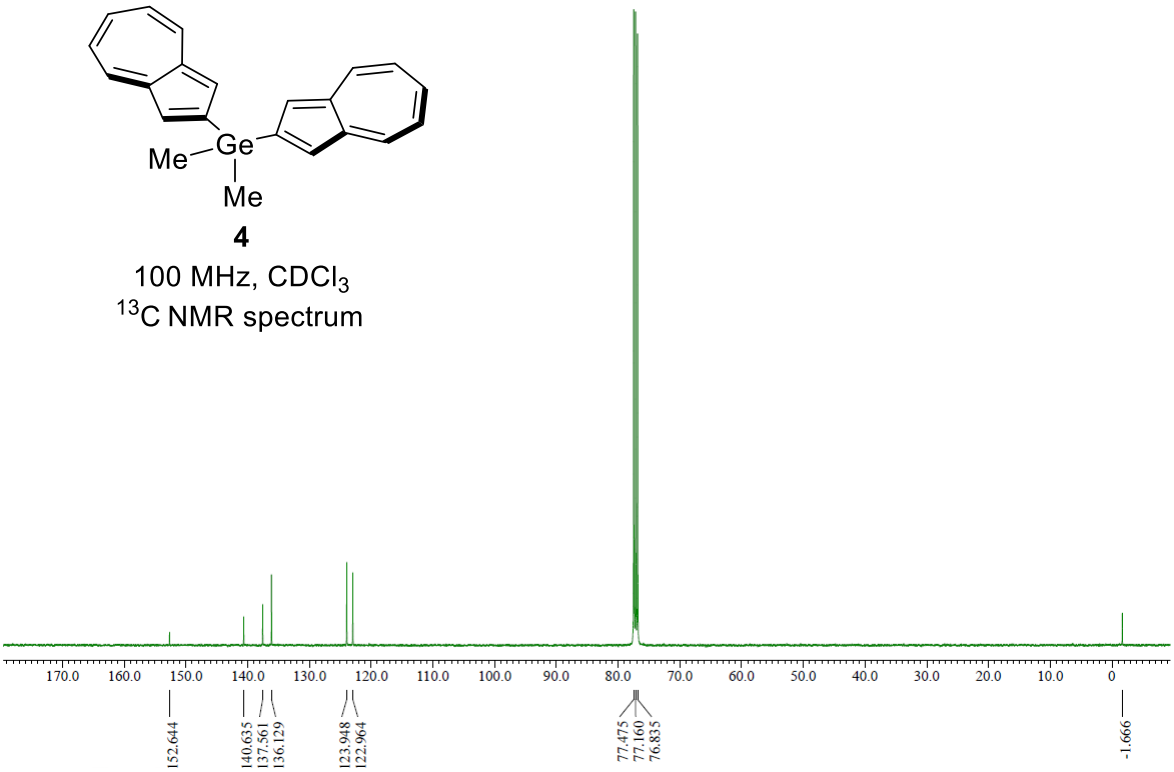

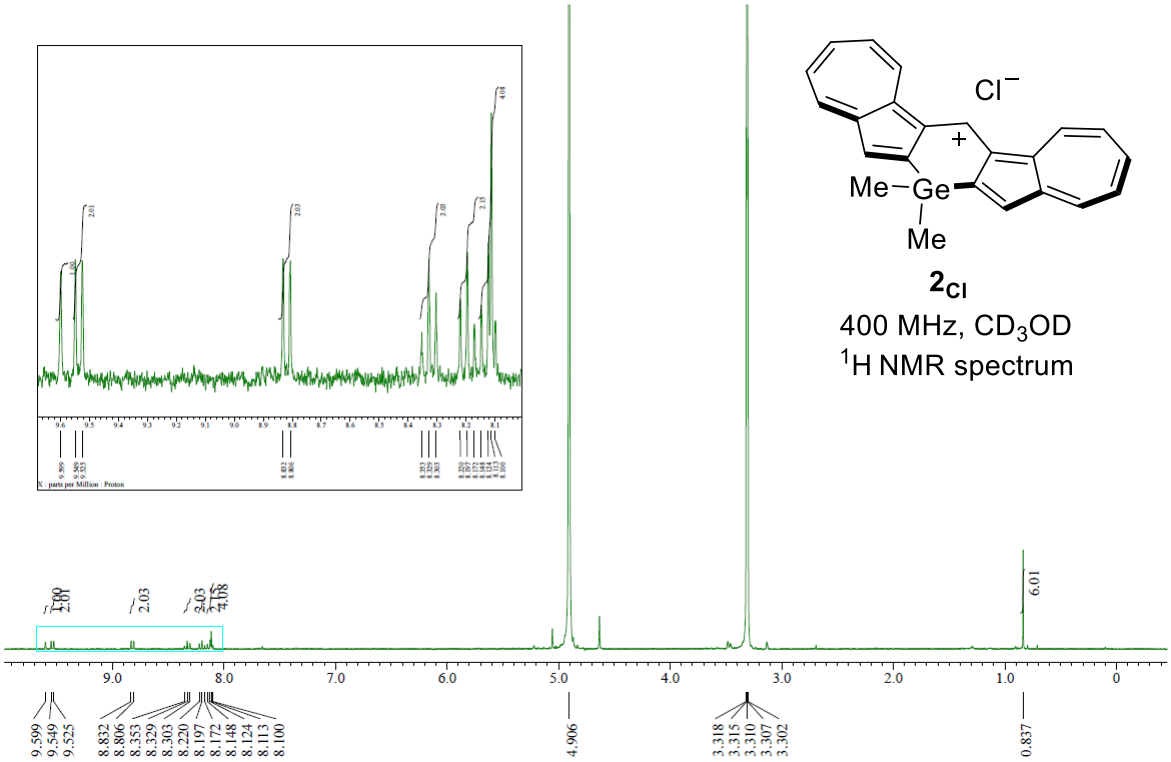

2_{Cl}
400 MHz, CD_3OD
^1H NMR spectrum

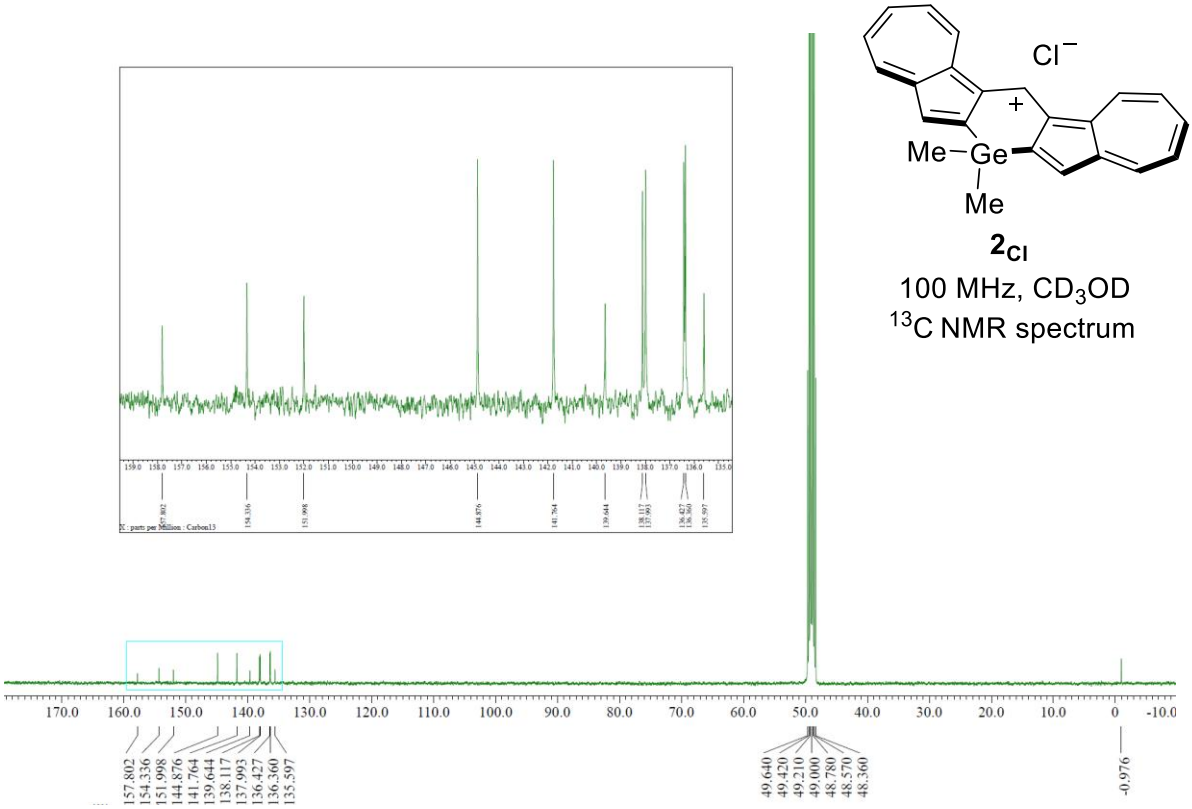

2_{Cl}
100 MHz, CD_3OD
^{13}C NMR spectrum

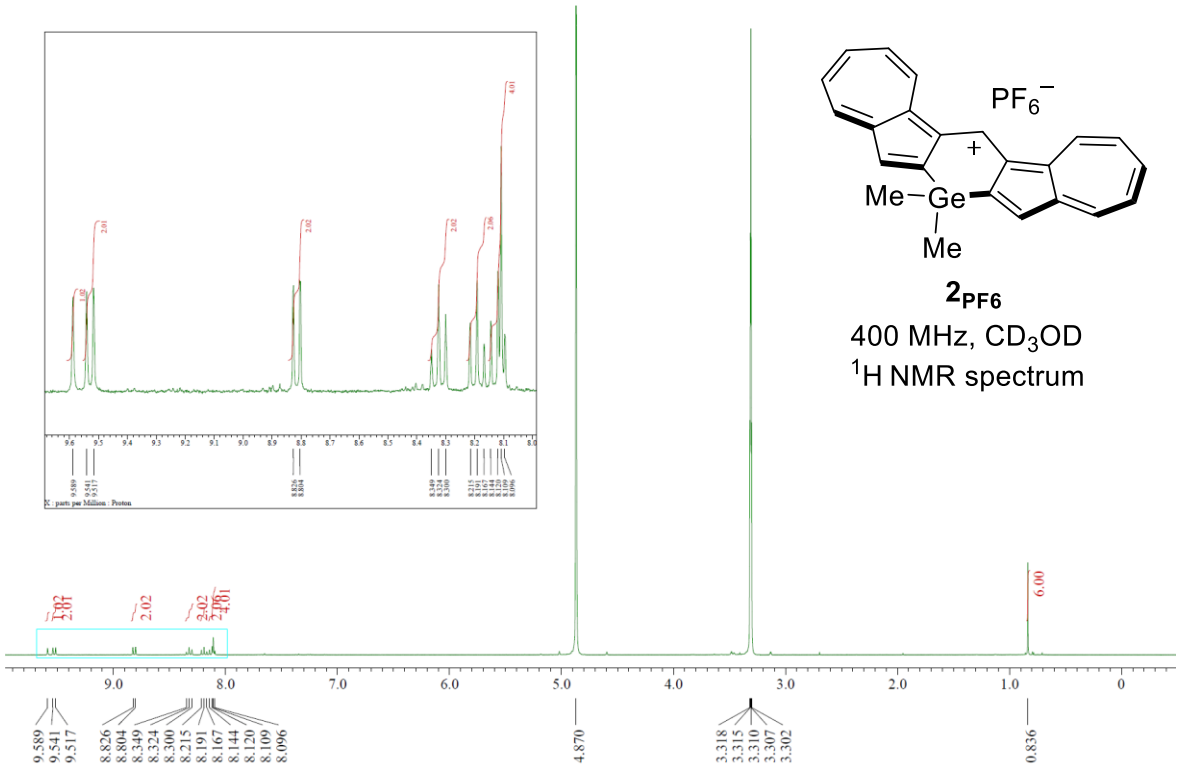
PF6−
+
Me−Ge
Me
2PF6
400 MHz, CD3OD
1H NMR spectrum

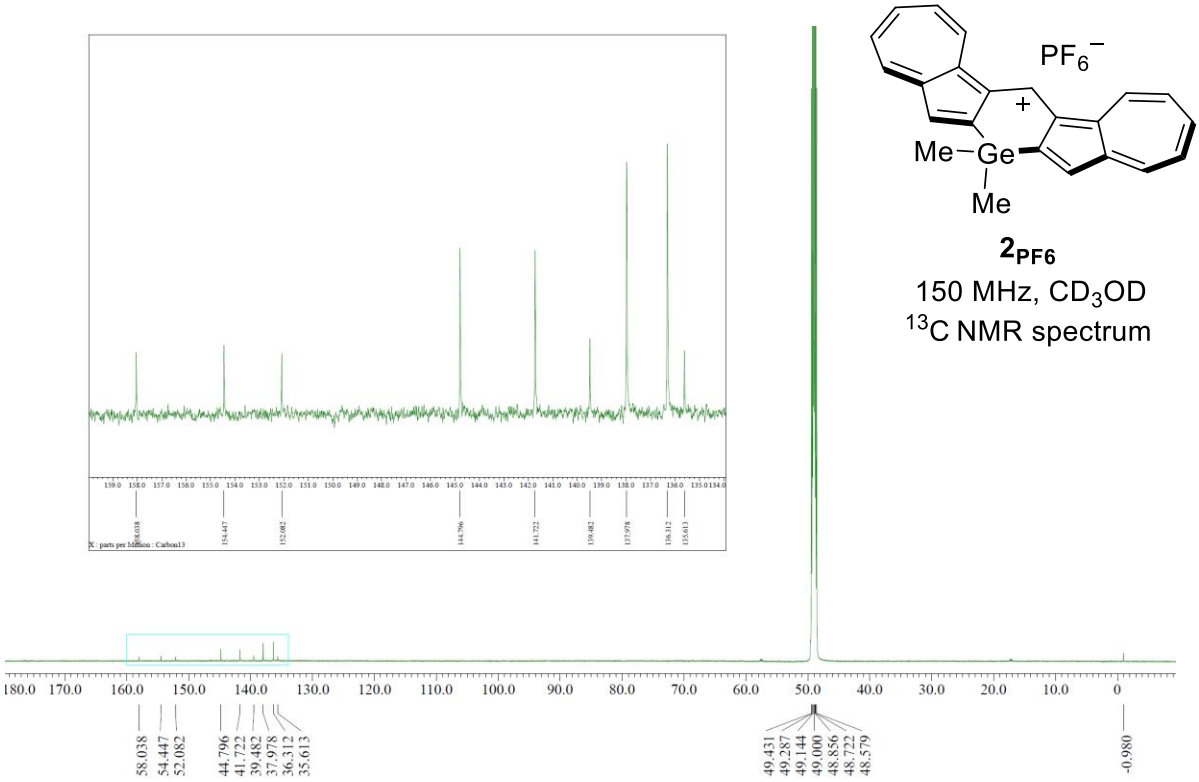
PF6−
+
Me−Ge
Me
2PF6
150 MHz, CD3OD
13C NMR spectrum

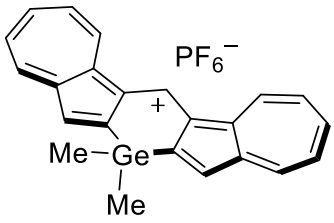

2PF6

376 MHz, CD_3OD

^{19}F NMR spectrum

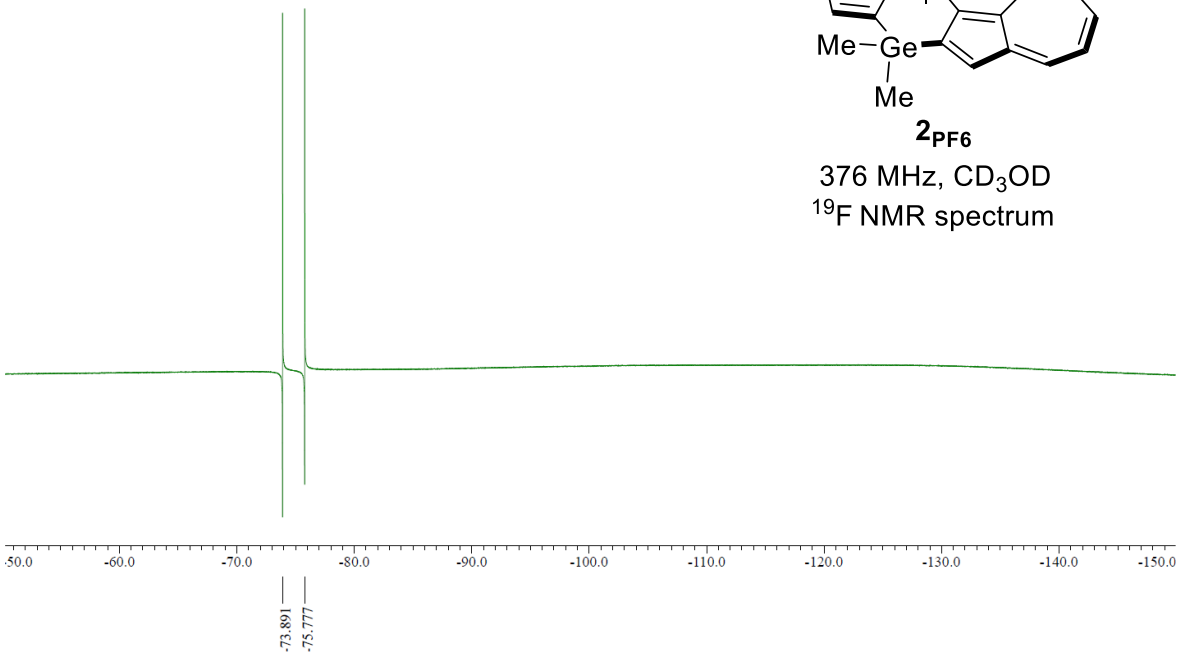

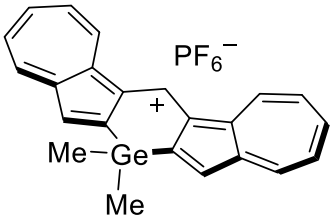

2PF6

162 MHz, CD_3OD

^{31}P NMR spectrum

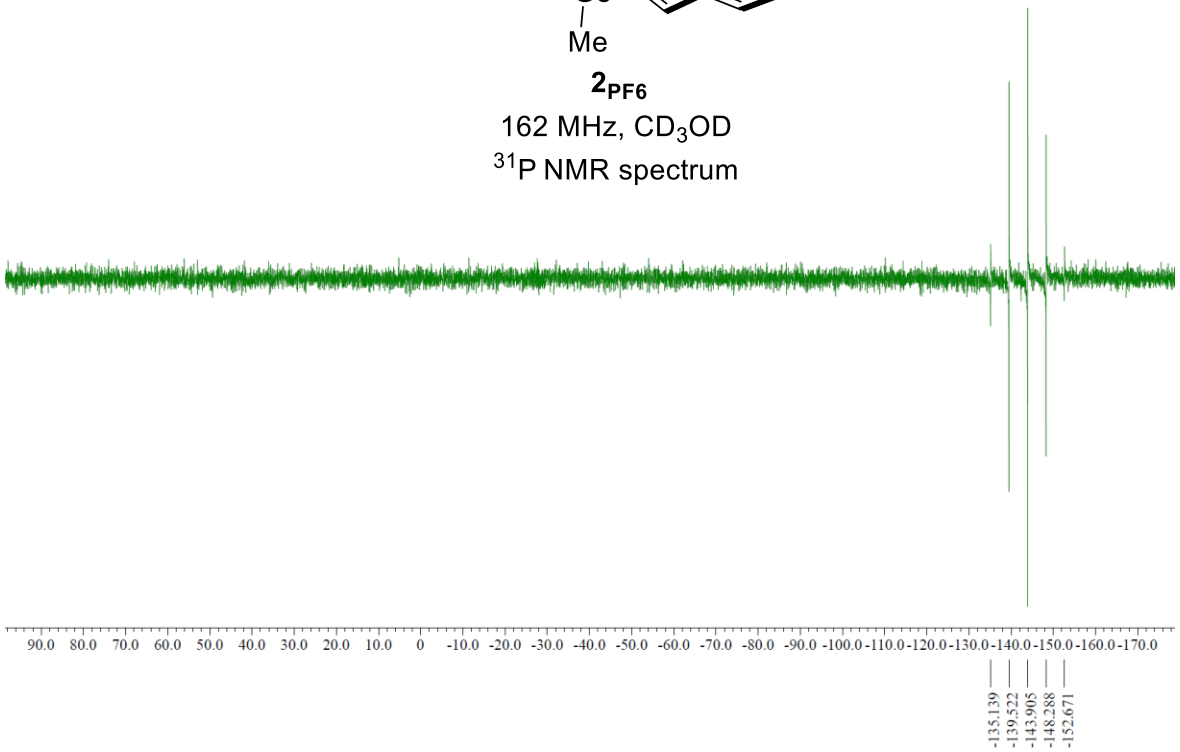

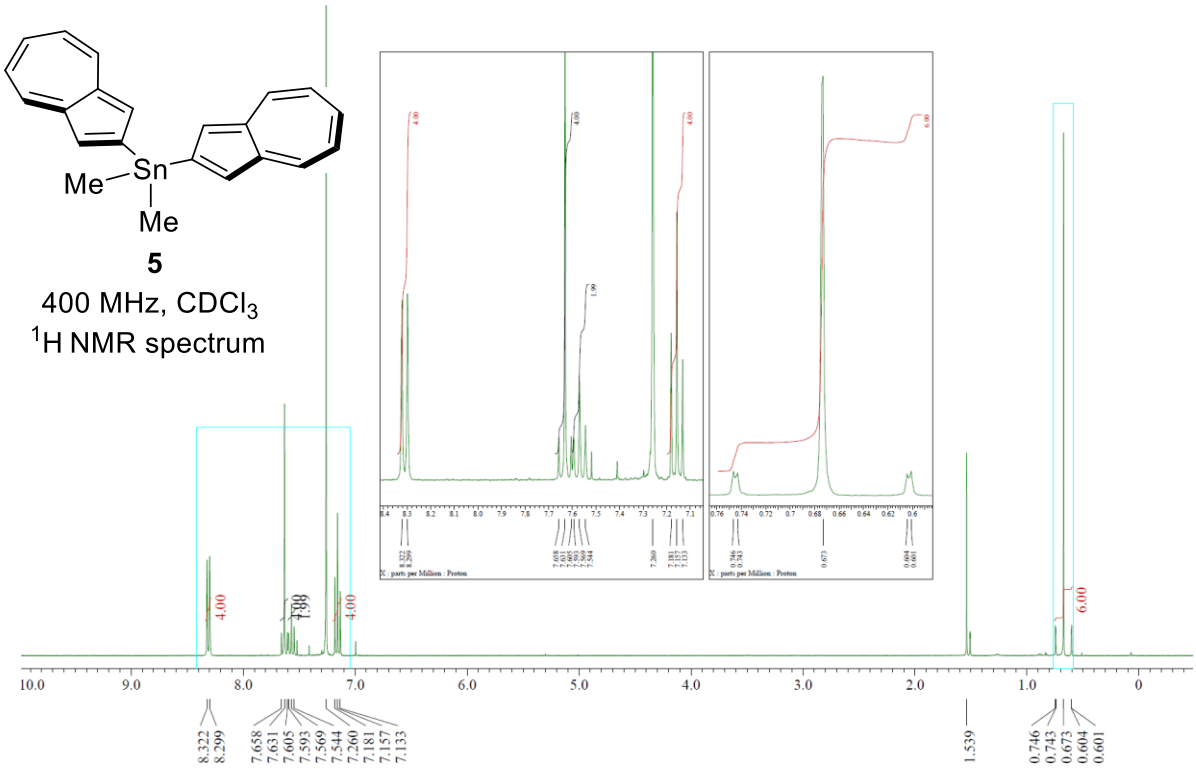
Me
Sn
Me
5
400 MHz, CDCl3
1H NMR spectrum
4.00
4.00
4.00
6.00
10.0
9.0
8.0
7.0
6.0
5.0
4.0
3.0
2.0
1.0
0
8.322
8.299
7.658
7.631
7.605
7.593
7.569
7.544
7.260
7.181
7.157
7.133
1.539
0.746
0.743
0.673
0.604
0.601

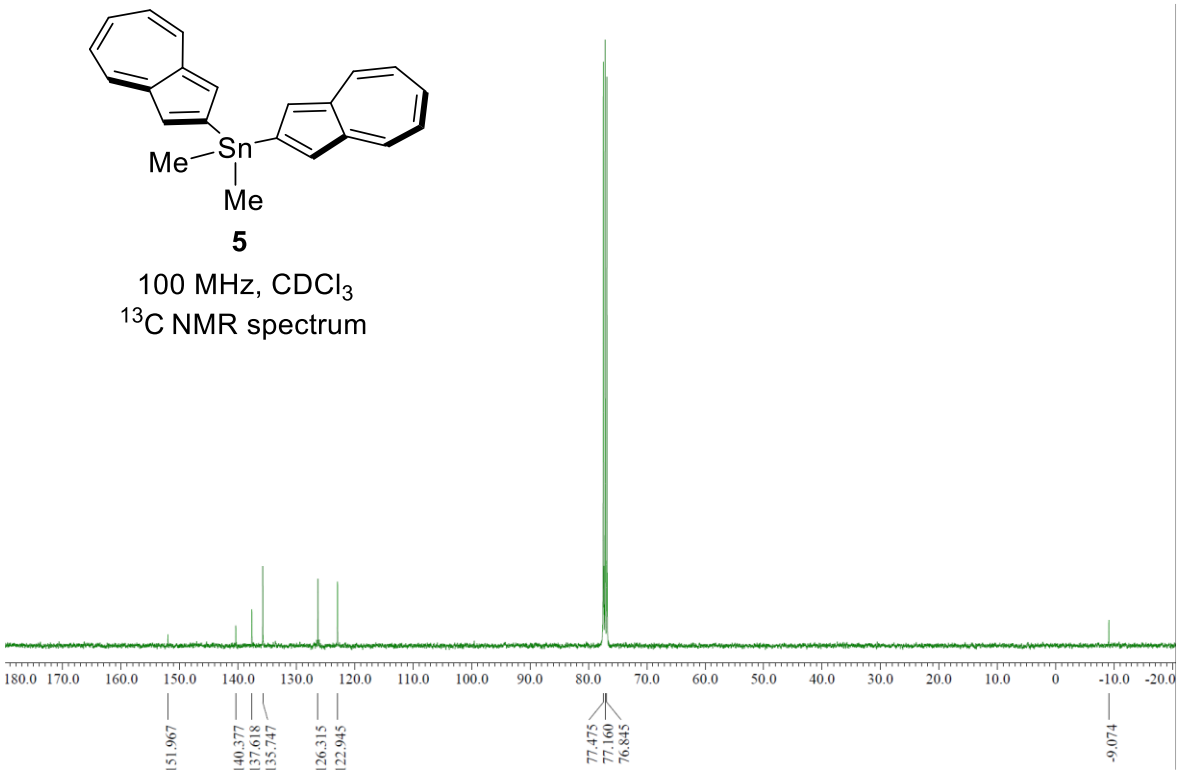
Me
Sn
Me
5
100 MHz, CDCl3
13C NMR spectrum
180.0
170.0
160.0
150.0
140.0
130.0
120.0
110.0
100.0
90.0
80.0
70.0
60.0
50.0
40.0
30.0
20.0
10.0
0
-10.0
-20.0
151.967
140.377
137.618
135.747
126.315
122.945
77.475
77.160
76.845
-9.074

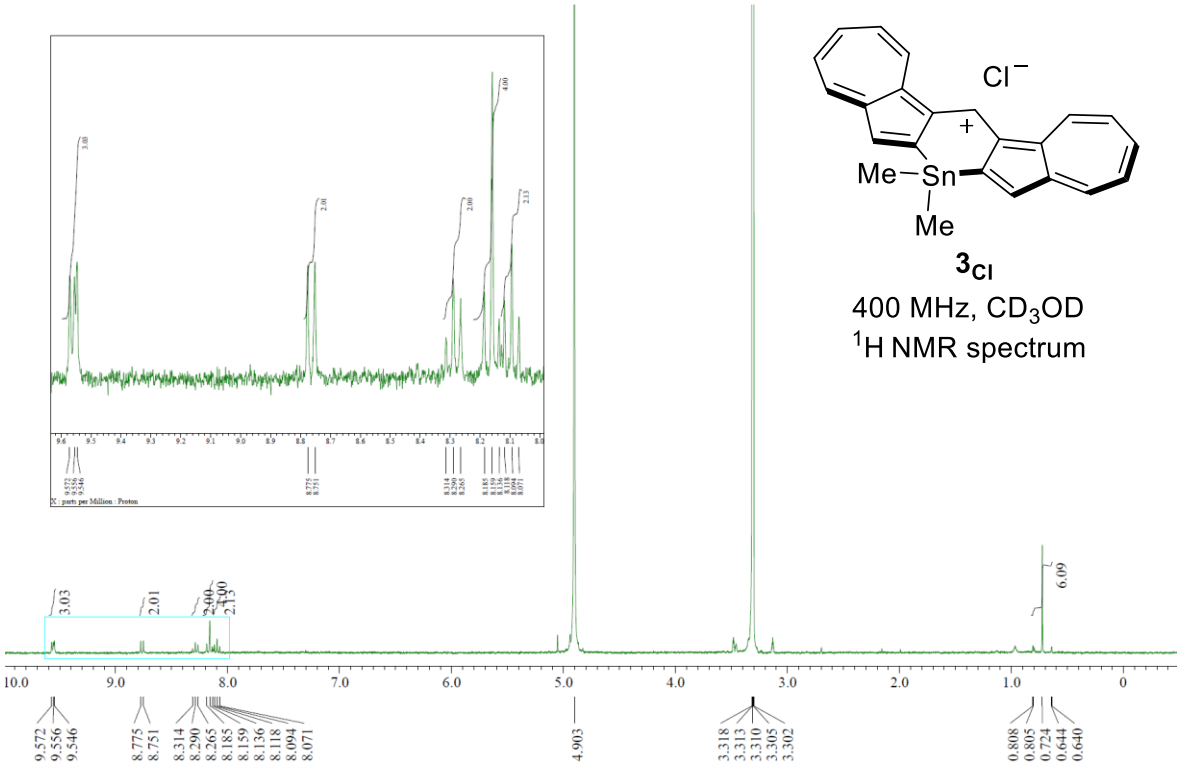

$\mathbf{3_{Cl}}$

400 MHz, CD_3OD

^{1}H NMR spectrum

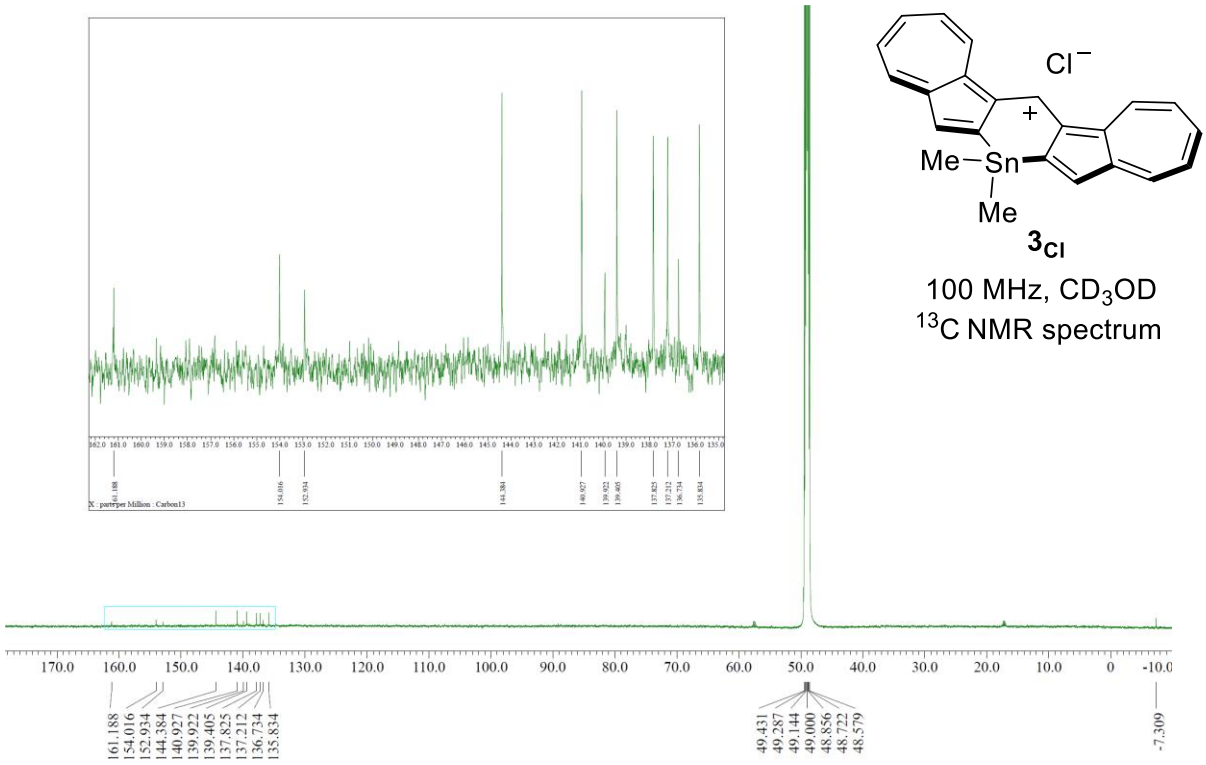

$\mathbf{3_{Cl}}$

100 MHz, CD_3OD

^{13}C NMR spectrum

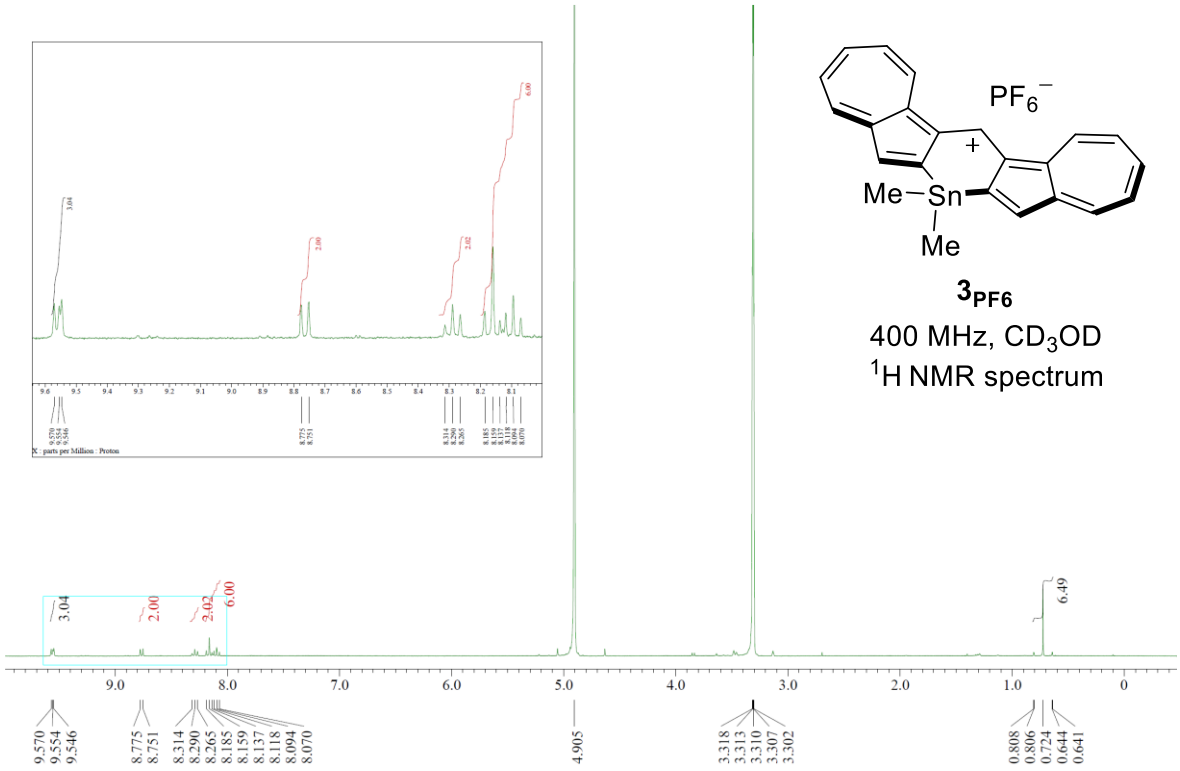

3_{PF6}

400 MHz, CD_3OD

^1H NMR spectrum

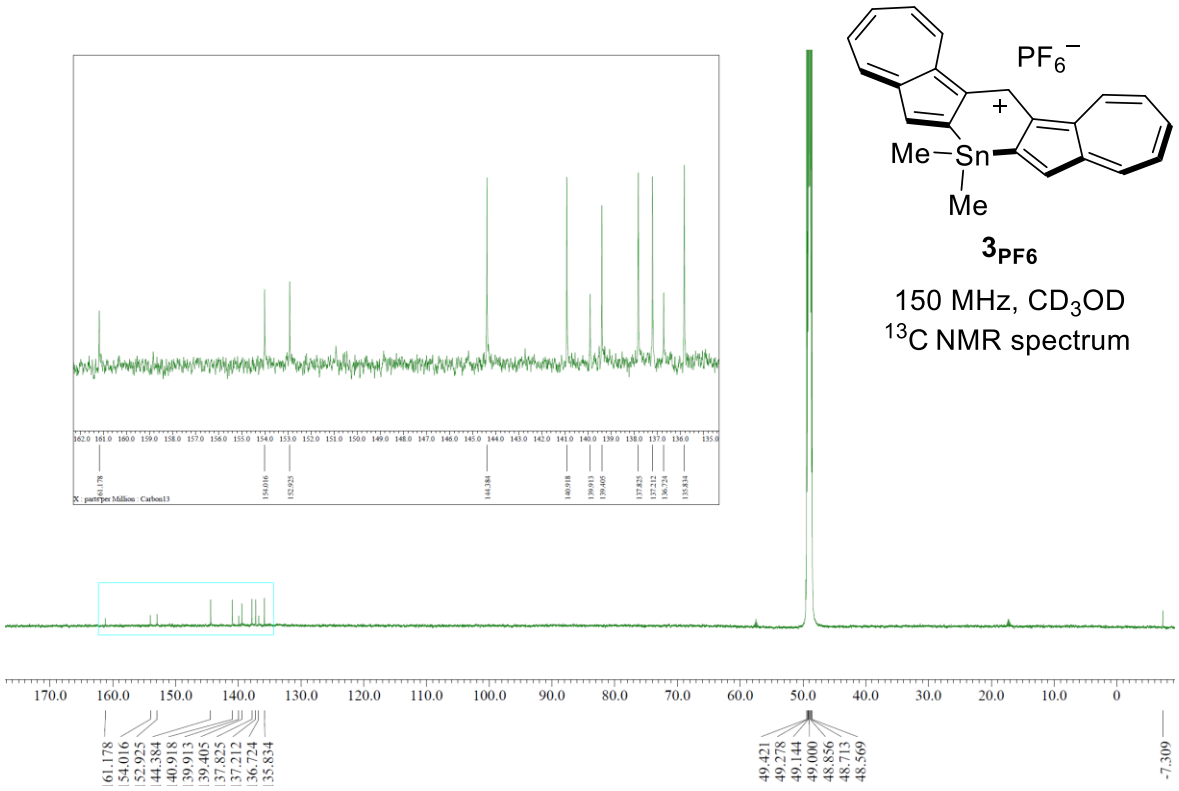

3_{PF6}

150 MHz, CD_3OD

^{13}C NMR spectrum

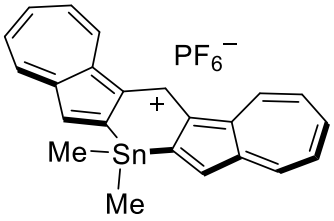

3PF6

376 MHz, CD_3OD

^{19}F NMR spectrum

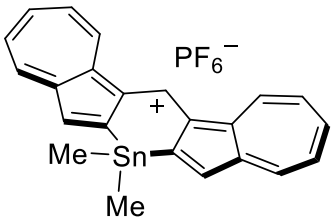

3PF6

162 MHz, CD_3OD

^{31}P NMR spectrum